Earth and Planetary Science Letters 530 (2020) 115922

Contents lists available at ScienceDirect

Earth and Planetary Science Letters

www.elsevier.com/locate/epsl

Temperature-enhanced electrical conductivity anisotropy in partially molten peridotite under shear deformation

Baohua Zhang [a,b,*], Takashi Yoshino [c]

[a] Institute of Geology and Geophysics, School of Earth Sciences, Zhejiang University, Hangzhou 310027, China
[b] Key Laboratory for High-Temperature and High-Pressure Study of the Earth's Interior, Institute of Geochemistry, Chinese Academy of Sciences, Guiyang, Guizhou 550081, China
[c] Institute for Planetary Materials, Okayama University, Misasa, Tottori-ken 682-0193, Japan

ARTICLE INFO

Article history:
Received 7 June 2019
Received in revised form 4 October 2019
Accepted 21 October 2019
Available online 5 November 2019
Editor: J. Brodholt

Keywords:
electrical conductivity anisotropy
partial melt
peridotite
shear deformation
high conductivity anomalies
oceanic asthenosphere

ABSTRACT

The high conductivity anomalies observed in the oceanic asthenosphere have shown anisotropic signature parallel to the plate motion. Anisotropic alignment of partial melt has been considered to one of probable explanations for the observed anisotropic conductivity structure, but the effect of temperature on the distribution of melt, the composition of melt, and the magnitude of electrical anisotropy for partial molten peridotite is unknown under shear deformation. In this study, the electrical conductivity of partially molten peridotite (KLB-1) under shear deformation was measured at 1 GPa in a DIA type apparatus with a uniaxial deformation facility to provide new constraints on the anisotropic signature in the oceanic asthenosphere. The conductivity measurements were performed simultaneously in two directions of three principal axes: parallel and normal to the shear direction on the shear plane, and perpendicular to the shear plane, by using impedance spectroscopy at temperature ranges of 1483-1548 K. Our results indicate that the total melt fraction, the absolute conductivity values, and the magnitude of electrical anisotropy of partially molten peridotite increase with increasing temperature. Although the Na_2O content varies widely at constant temperature in the recovered melt, very small changes of shear-parallel conductivities (σ_x) before and after shear deformation suggest that the electrical conductivity of partially molten peridotite is mainly controlled by temperature, rather than alkali content in partial melt. Microstructural observations of the recovered samples reveal that the development of conductivity anisotropy was caused by the realignment of melt pockets parallel to the shear direction, which forms two melt-rich regions. Furthermore, we estimate how much melt fraction is partitioned into melt-rich regions by calculating the area ratio of two melt-rich regions to the whole area. Our calculations show that once melt segregation occurs, more than 50% of the total melt fraction will partition into the melt-rich regions, and this proportion will continue to increase with the increase of temperature. This finding suggests that development of electrical anisotropy in partially molten peridotite under shear deformation will increase with increasing temperature, which may provide new constraints on interpretation of high conductivity anomalies observed in the oceanic asthenosphere.

1. Introduction

Anisotropic feature of electrical conductivity observed from magnetotelluric data in the asthenosphere just below the lithosphere-asthenosphere boundary (LAB) (Evans et al., 2005; Baba et al., 2006; Naif et al., 2013) has been attributed to the presence of hydrous olivine (Karato, 1990; Wang et al., 2006) and/or of partial melting of peridotite (Gaillard et al., 2008; Yoshino et al., 2006, 2010; Yoshino and Katsura, 2013; Sifré et al., 2014). Remarkably, Dai and Karato (2014) reported new electrical conductivity measurements on oriented single crystals of hydrous olivine showing a higher increase in conductivity and conductivity anisotropy at high temperature than previously investigated. Subsequently, after reanalyzing Dai and Karato's data, Gardés et al. (2015) raised a number of criticisms of Dai and Karato (2014) and concluded that this new study does not extend but restricts the magnitude of olivine conductivity enhancement by water. Thus, a small anisotropic conductivity of single crystal hydrous olivine (Yoshino et al., 2006; Poe et al., 2010; Yang, 2012) verifies the implausi-

* Corresponding author at: Institute of Geology and Geophysics, School of Earth Sciences, Zhejiang University, Hangzhou 310027, China.
E-mail addresses: zhangbaohua@zju.edu.cn, zhangbaohua@vip.gyig.ac.cn (B. Zhang).

https://doi.org/10.1016/j.epsl.2019.115922
0012-821X/

bility of proton conduction in olivine for explanation of the high conductivity anisotropy observed in the asthenosphere near the Eastern Pacific Rise. Experimental investigations have shown that the presence of partial melt can trigger high conductivity (Gaillard et al., 2008; Yoshino et al., 2010; Ni et al., 2011; Sifré et al., 2014; Laumonier et al., 2017). Under quasi-hydrostatic condition, the equilibrium melt distribution predicted from the interfacial energy minimization is isotropic. To explain the geophysically observed anisotropic feature, many workers have proposed that the conductivity anomaly features are caused by the anisotropic redistribution of melt in partially molten rocks under shear deformation (Holtzman et al., 2003; Holtzman and Kohlstedt, 2007; Kohlstedt and Holtzman, 2009; Caricchi et al., 2011; Zhang et al., 2014; Pommier et al., 2015).

The generation of channel-like melt-enriched structures with high degree of melt connectivity in the spreading direction coupled with low connectivity in the ridge parallel direction has been proposed to account for the electrical anisotropy and seismic wave velocity reduction at the LAB underneath oceanic plates (Holtzman et al., 2003; Weeraratne et al., 2007; Kohlstedt and Holtzman, 2009; Caricchi et al., 2011). This unique melt distribution is usually attributed to mantle deformation that can attribute to the motion of rigid lithospheric plates relative to the underlying convection mantle (Kawakatsu et al., 2009). The quantitative interpretation of such an anisotropic structure revealed by magnetotelluric profiles requires robust laboratory characterization under controlled conditions. The magnitudes of the seismic velocity and conductivity variations are directly linked to the melt fraction, therefore comparison of geophysical data with laboratory models has long been considered as the most plausible way to quantify the melt contents in partially molten regions of the Earth (Shankland and Waff, 1977). So far, only two studies have addressed the electrical conductivity of partially molten peridotite under shear deformation (Caricchi et al., 2011; Zhang et al., 2014). Caricchi et al. (2011) firstly reported reduction of electrical conductivity normal to shear direction during deformation of melt-bearing olivine aggregates in torsion and implied that the conductivity anisotropy observed in the asthenosphere can be explained by the flow-aligned tube-like structure of melt. However, this study did not simultaneously measure conductivity in the directions parallel and normal to shear direction, and contains both large shear strain and stress gradients along the conductivity measurement direction. Zhang et al. (2014) simultaneously measured the electrical conductivity of olivine + chromite/enstatite aggregates with basaltic melts in two directions of three principal axes: parallel and normal to the shear direction on the shear plane, and perpendicular to the shear plane. They concluded that the sheared peridotite analog with 2 vol.% of partial melt can well explain the geophysical observations.

Pommier et al. (2015) reported new results of laboratory measurements on the electrical conductivity of pre-deformed partially molten samples with large strain ($1.2 < \gamma < 9$) and claimed that the electrical anisotropy of the asthenosphere could be reproduced by an electrical layered model either sheared Fo_{90} + 5 vol.% MORB or Fo_{90} + 2 vol.% carbonated melt. However, Pommier et al. (2015) performed the electrical conductivity measurements at high temperatures under quasi-hydrostatic condition but not under shear deformation. Their experimental set-up and condition are unlikely to evaluate the effect of shear deformation on the whole process of conductivity anisotropy evaluation in partially molten systems.

Although all of these previous experimental findings provided some constraints on the observed conductivity anisotropy, there have been still several problems which are needed to be clarified further: (1) To simplify the experimental complexity in previous studies, the starting materials were olivine + melt (basalt or carbonatite). However, a widely accepted composition model of the MORB source's mantle (Ringwood, 1975; Takahashi, 1986) is fertile peridotitic composition. At the fixed bulk composition, melt composition and wetting behavior can vary with increasing temperature and pressure (Yoshino et al., 2009). To better understand the high conductivity anomalies revealed by MT surveys in the upper mantle, we need to determine the three-dimensional (3D) electrical conductivity of partially molten peridotite under shear deformation. (2) In-situ conductivity measurement on partially molten system is an effective way to constrain possible melt distribution at the top of the oceanic asthenosphere. Under quasi-hydrostatic conditions, many studies (e.g., Gaillard et al., 2008; Yoshino et al., 2010; Ni et al., 2011; Sifré et al., 2014; Laumonier et al., 2017) have investigated the effect of melt fraction on the electrical conductivity of partial molten peridotite. For example, Laumonier et al. (2017) interpreted the upper asthenosphere electrical anomaly to result from the presence of 0.5-1.0 vol.% melt, and argued that anisotropic distribution of the melt is not necessarily required in order to explain high conductivities observed in the upper mantle settings. In contrast, recent shear deformation experiments (Caricchi et al., 2011; Zhang et al., 2014) revealed that development of electrical anisotropy is caused by anisotropic distribution of the melt. One of important features of these studies is that once melt distribution is highly anisotropic, the melt fraction may no longer be an important influencing factor on the electrical anisotropy. Knowledge of melt distribution to produce the anisotropic conductivity in the oceanic asthenosphere rather than discussion on melt fraction is necessary to constrain the conductivity and seismic features under shear deformation of partial molten peridotite. Melt distribution also would vary with melt fraction as a function of temperature under shear deformation. Thus knowledge of electrical conductivity of peridotite with more realistic composition should be required to figure out the above issues.

In this study, we conducted in situ electrical conductivity measurements acquired on partially molten peridotite with KLB-1 composition at various temperatures and strain rates. We investigate the effects of melt distribution, temperature, melt fraction, annealing time, strain and strain rate on the electrical conductivity anisotropy. The present experiments will provide new constraints on the potential melt fraction in the oceanic upper mantle.

2. Experimental and analytical techniques

2.1. Sample preparation

We used fertile peridotite with KLB-1 composition as the starting material for this study. KLB-1 represents a typical fertile mantle peridotite, its composition is proposed to represent the undepleted and primitive composition of the Earth's mantle as documented by Takahashi (1986). The starting material with the KLB-1 peridotite composition was prepared from a mixture of SiO_2, TiO_2, Fe_2O_3, Al_2O_3, MnO, MgO, NiO, Cr_2O_3, $CaCO_3$, Na_2CO_3 and K_2CO_3 in the following procedure. Before weighed, the oxide powders and carbonates were dried at 1273 K and 473 K for 12 hours, respectively, then mixed and ground in an agate mortar. These mixtures were pressed into pellets and then decarbonated at 1233 K. The recovered products were finely ground and pressed into pellets again. The pellets were heated in a gas-controlled furnace at 1393 K for one hour with controlled oxygen partial pressure of $\log f O_2 = -9.477$ [log atm], which is close to the QFM buffer, and then quenched into water. The peridotite samples were synthesized in an end-loaded piston-cylinder apparatus at a pressure of 1 GPa and a temperature of 1473 K (below the sub-solidus temperature) with 3/4″ pressure assemblies, for durations up to 5 hours. Finally, the samples were cooled to room temperature with a cooling rate of about 20 °C/min, which allowed us to obtain well sintered samples without cracking due to thermal shock. The

Table 1
Average melt composition of run products.

Run#	SiO_2	TiO_2	Al_2O_3	Cr_2O_3	FeO*	MnO	MgO	CaO	Na_2O	K_2O	Total
KLB-1†	44.48	0.16	3.59	0.31	8.10	0.12	39.22	3.44	0.30	0.02	99.74
A2598 (N = 9)	55.07 (1.01)	0.84 (0.03)	14.83 (0.15)	0.11 (0.03)	4.55 (0.13)	0.28 (0.05)	7.76 (0.30)	14.39 (0.26)	2.09 (0.14)	0.19 (0.04)	100.11 (0.52)
A2544 (N = 10)	54.60 (0.44)	0.79 (0.01)	13.78 (0.11)	0.13 (0.01)	5.45 (0.09)	0.25 (0.02)	7.92 (0.21)	13.54 (0.16)	2.55 (0.13)	0.16 (0.02)	99.18 (0.73)
A2545 (N = 13)	53.77 (0.31)	0.68 (0.02)	13.91 (0.10)	0.10 (0.02)	5.69 (0.11)	0.26 (0.04)	9.22 (0.17)	13.31 (0.22)	2.35 (0.11)	0.15 (0.03)	99.44 (0.51)
A2548 (N = 12)	53.16 (0.41)	0.71 (0.03)	12.68 (0.13)	0.15 (0.01)	5.39 (0.13)	0.23 (0.05)	10.78 (0.23)	12.72 (0.16)	2.17 (0.12)	0.17 (0.01)	98.16 (0.86)
A2549 (N = 14)	53.88 (0.38)	0.65 (0.04)	12.81 (0.16)	0.16 (0.02)	6.15 (0.06)	0.25 (0.02)	11.34 (0.22)	12.52 (0.22)	1.91 (0.08)	0.16 (0.02)	99.83 (0.45)
A2599 (N = 11)	52.99 (0.41)	0.61 (0.03)	12.11 (0.18)	0.14 (0.03)	6.83 (0.18)	0.24 (0.06)	12.50 (0.31)	11.89 (0.21)	1.79 (0.13)	0.15 (0.04)	99.25 (0.56)
A2600 (N = 13)	50.87 (0.37)	0.57 (0.02)	11.57 (0.12)	0.16 (0.02)	7.68 (0.12)	0.23 (0.04)	13.15 (0.22)	10.54 (0.25)	2.19 (0.11)	0.13 (0.02)	97.09 (0.85)
A2602 (N = 18)	50.20 (0.29)	0.55 (0.03)	11.30 (0.09)	0.18 (0.01)	7.38 (0.09)	0.26 (0.02)	14.59 (0.13)	10.03 (0.12)	1.92 (0.11)	0.14 (0.03)	96.55 (0.31)
A2558 (N = 16)	49.95 (0.34)	0.46 (0.04)	10.21 (0.16)	0.17 (0.01)	8.44 (0.11)	0.24 (0.05)	17.87 (0.18)	9.41 (0.20)	1.77 (0.08)	0.09 (0.01)	98.61 (0.75)
A2601 (N = 15)	49.90 (0.53)	0.42 (0.05)	10.30 (0.13)	0.19 (0.03)	8.69 (0.16)	0.22 (0.07)	18.73 (0.26)	9.35 (0.25)	1.26 (0.07)	0.07 (0.01)	99.13 (0.68)

All experiments were conducted at 1 GPa.
† Chemical composition of KLB-1 peridotite (Takahashi, 1986).
Note that average compositions of randomly selected melt areas for each sample were determined by EPMA and are given in wt.%. *N* denotes numbers of analysis and number in parentheses are 1σ deviation from the mean. FeO* = Total Fe as FeO.

Table 2
Summary of experimental conditions.

Run no.	T (K)	ϕ	d (mm)	L (μm)	υ (μm/h)	t (min)	γ	$\dot{\gamma}$ (s^{-1})	$\Delta(\log\sigma)$[a]	Remarks[b]
A2544	1498	0.018	0.56	800	150	305	0.78	4.26×10^{-5}	0.71	Const. P
A2545	1498	0.020	0.50	705	70	420	1.11	4.41×10^{-5}	0.72	Decrease P
A2548	1498	0.019	0.58	1004	200	250	1.22	8.13×10^{-5}	0.82[c]	Decrease P
A2549	1498	0.021	0.62	645	50	550	0.68	2.06×10^{-5}	0.80[c]	Const. P
A2558	1548	0.058	0.37	1005	100	450	1.75	6.48×10^{-5}	0.99[c]	TC control
A2598	1483	0.014	0.51	1107	150	300	0.66	3.67×10^{-5}	0.55	Const. P
A2599	1508	0.032	0.46	938	100	420	1.30	5.16×10^{-5}	0.61	TC control
A2600	1523	0.042	0.66	662	70	360	0.83	3.84×10^{-5}	0.64	TC control
A2601	1548	0.061	0.64	483	50	350	1.05	5.00×10^{-5}	0.86[c]	Const. P
A2602	1523	0.040	0.60	1546	300	220	0.92	6.97×10^{-5}	0.74	TC control

All experiments were conducted at 1 GPa.
Abbreviations: ϕ, melt fraction after shear deformation; d, sample thickness; L, displacement; υ, displacement rate of the differential piston; t, effective time; γ, final shear strain; $\dot{\gamma}$, shear strain rate.
[a] Conductivity anisotropy is defined as $\Delta(\log\sigma) = \log\sigma_x - \log\sigma_y$.
[b] Method to maintain constant temperature. Const. P: constant power; Decrease P: slightly decreased power during deformation; TC control: thermocouple control.
[c] Conductivity anisotropy is defined as $\Delta(\log\sigma) = \log\sigma_x - \log\sigma_z$.

chemical compositions of starting materials and quenched melt in run products are listed in Table 1.

2.2. In situ conductivity measurements under shear deformation

In-situ electrical conductivity of partially molten peridotite were measured simultaneously in two directions of three principal axes: parallel and normal to the shear direction on the shear plane, and perpendicular to the shear plane in a DIA-type apparatus during shear deformation under high temperature and high pressure. All the details about the DIA-type apparatus and the cell assembly for in situ conductivity measurement can be found in Zhang et al. (2014). In this study, the same method was applied to measure the electrical conductivity of the peridotite. We investigated the effects of temperature, strain and time on the melt redistribution and the development of conductivity anisotropy during shear deformation. The pressure was calibrated using phase transition of Bi (2.5 and 7.7 GPa) at ambient temperature and SiO_2 (quartz to coesite) at high temperature. Taking into consideration of a slight pressure drop by heating and cooling, thus the error of pressure estimation is around ±0.2 GPa.

All conductivity measurements were performed at a confining pressure of 1 GPa and various temperatures (1483–1548 K) (Table 2), using a Solartron 1260 Impedance/Gain-Phase Analyzer (combined with a Solartron 1296 Interface if the sample resistance was higher than MΩ). The complex impedance spectra were obtained over frequencies ranging from 10^6 to 10^{-1} Hz under AC voltage with an amplitude of 1 V. The experimental strategy for electrical conductivity measurement of the sample under shear was as follows: (1) The sample was first pressurized to the desired pressure (1 GPa) and then followed by heating (this period is defined as t_1 in Appendix A). (2) During heating, the electrical conductivity of the sample was measured at 100 K interval until the sample was heated up to the target temperatures. Initial melting of sample is characterized by a drastic decrease in the sample resistance (increase in conductivity) (Fig. S1) and then temperature was kept at the constant target temperature for more than 2 hours to achieve the texture equilibrium (t_2). During annealing, the conductivity was frequently monitored to identify establishment of the equilibrium melt distribution (see Fig. S1 in Supplementary Material). (3) Once the conductivity was found to become stable at the desired temperature, the tungsten carbide (WC) piston started advancing from the zero time in Fig. 1a. In the initial stage of shear deformation, although a higher displacement rate (for example run A2549 in Fig. 1a, we set a step-by-step decreasing rate: 300 μm/h for 10 min → 200 μm/h for 20 min → 100 μm/h for 30 min → 50 μm/h) of the differential piston was set compared with the final constant displacement rate, it is found that both actual speed (displacement rate) and actual displacement became negative before positive with increasing actual load (Fig. 1a). When the actual displacement increases from zero (time = 105 min at point 1 in Fig. 1a, this period is t_3), we believe the "hit position" was accomplished for the inner WC piston in the DIA-type apparatus. Therefore, the time corresponding to the point 1 or "hit position" is considered to the beginning time of real shear deformation. (4) Samples were deformed by advancing the piston with a constant displacement rate between 50 and 300 μm/h, and simultaneous conductivity measurements of the partially molten peridotite in *x*

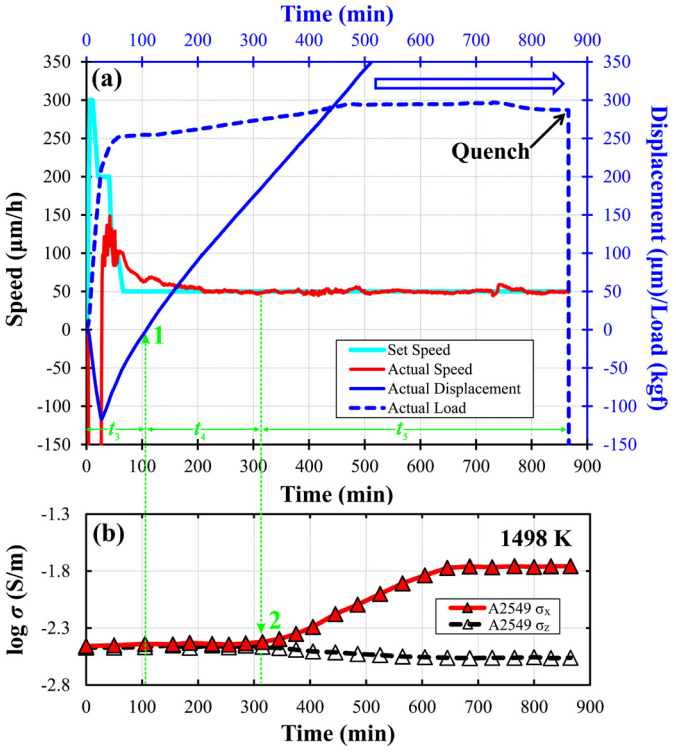

Fig. 1. Variation of displacement rate (speed), displacement and load (a), and electrical conductivity (b) with increasing time for run A2549 at 1498 K. Note that, the time t_1 to t_5 have been defined and explained in text and Appendix A. (For interpretation of the colors in the figures, the reader is referred to the web version of this article.)

and y (or z) directions were conducted every 20 min during shear deformation. With the accumulation of stress and the increase of strain, conductivity anisotropy begins to appear at point 2 (time = 315 min after onset of the inner WC piston advancement, t_4 is defined between point 1 and point 2) in Fig. 1b due to pronounced anisotropic melt redistribution. Thus, the time corresponding to the point 2 in this study was hereafter defined as "zero time" of effective time (t_5) for shear deformation. (5) After the shear deformation and conductivity measurements were completed, the sample was quenched in order to "freeze" the partially molten textures and then pressure was returned to atmospheric pressure. Temperature was controlled by WRe_3-WRe_{25} thermocouple or estimated by a relation between applied power and temperature (Zhang et al., 2014) when the thermocouple was broken. Uncertainties on the sample conductivity arise from sample geometry, temperature measurement and deviation during measurement, which are estimated to be less than 0.2 log units. The experimental conditions are summarized in Table 2.

2.3. Analytical techniques and imaging

The recovered samples were mounted in epoxy and cut along the direction perpendicular to the shear plane. The cross-section was then polished. Scanning electron microscopy (SEM) imaging and electron microprobe analyses (EPMA) were performed to characterize the texture and chemistry of each sample. The chemical composition of melt and mineral phases were obtained with focused (1 μm) beams using a JEOL JXA-8800 Electron Probe Microanalyzer at the Institute for Planetary Materials (IPM), Okayama University, with an acceleration voltage of 15 kV and beam current of 12 nA. To determine the melt fraction precisely and to characterize the alignment and distribution of melt phase in the partially molten peridotite quantitatively, we used the following method to

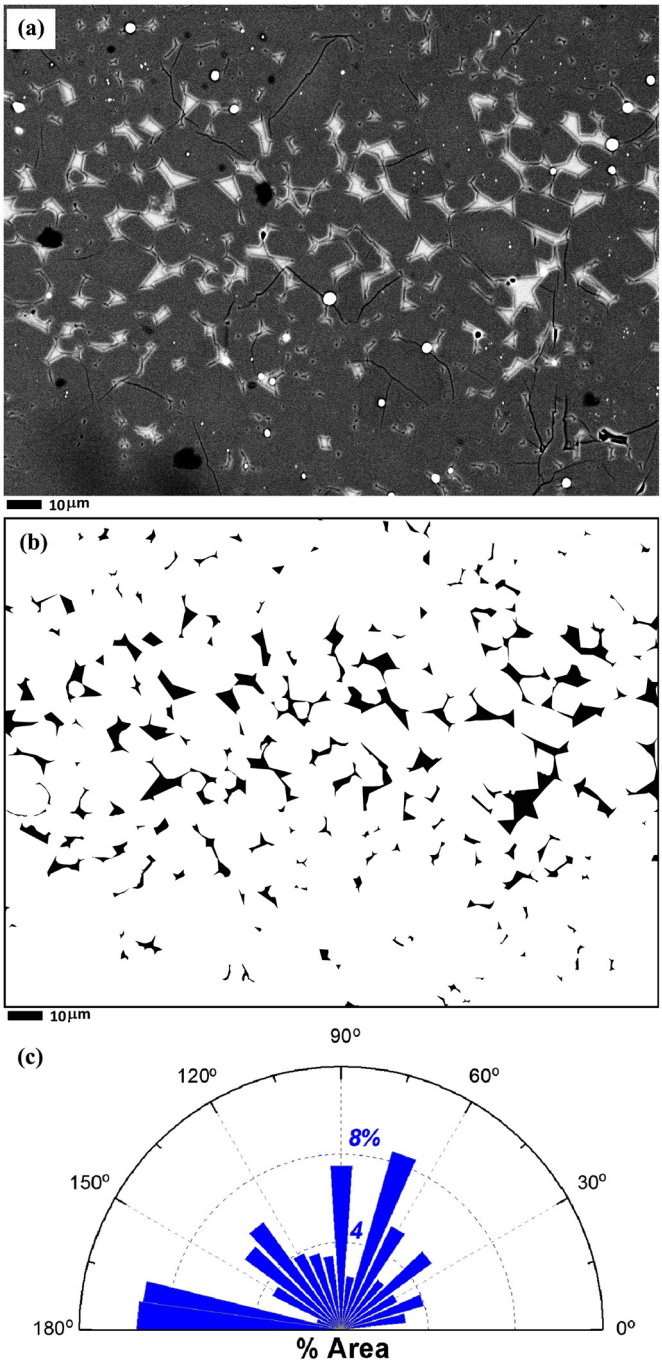

Fig. 2. Example of analytical procedures on experimental product. (a) Back scattered electron image of the deformed partially molten KLB-1 peridotite (A2601). (b) Traced melt pools from the area (a). (c) Orientation of the long axis of melt pockets (MPO) as a percentage of the total melt area when viewed in a section cut parallel (xz plane) to the shear direction.

estimate melt fraction and define melt distribution (more details about the methods in Supplementary Material). Image analysis on back-scattered electron (BSE) images from two different polished sections cut parallel (xz plane) and normal (yz plane) to the shear direction for each deformed sample was performed. The outlines of melt pockets were carefully traced by Adobe Illustrator on the screen to create binary images (Yoshino et al., 2005) as shown in Fig. 2. The long axis of melt pockets was obtained by elliptical determination. The area of each phase was determined by counting the number of pixels it occupied. To characterize variation of the melt fraction across the sheared sample, image analyses were also

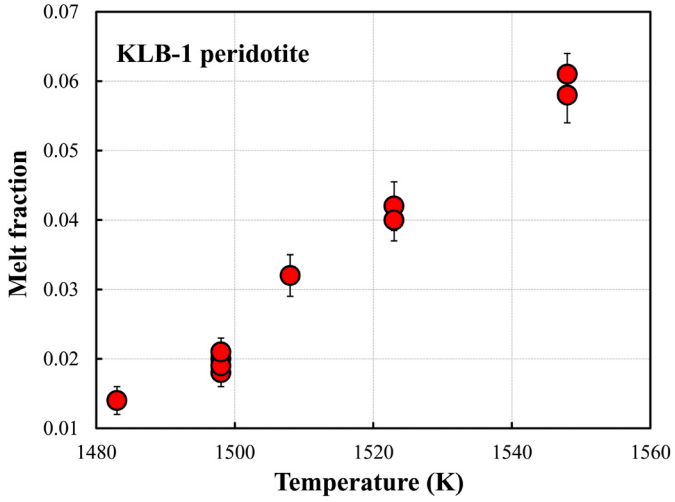

Fig. 3. The total melt fraction of KLB-1 peridotites as a function of temperature.

performed using the method proposed by Caricchi et al. (2011) and Zhang et al. (2014) because melt is heterogeneously distributed in the sheared sample. The analyzed area covered the whole polished surface of the sample. The amount of melt was measured each bin rectangular with 3 μm interval parallel to the shear direction across the shear plane. These data were converted into the frequency distribution of melt fraction along the z direction (Zhang et al., 2014). Finally, the total melt fraction of deformed samples was estimated from the whole polished surface including melt-free and melt-rich regions by means of the above-mentioned method.

3. Results

3.1. Effects of temperature and deformation on the electrical conductivity

The degree of melting of peridotite can be controlled by experimental temperature condition at fixed pressure. Because conductivity measurements were performed above the solidus temperature of the anhydrous KLB-1 peridotite (slightly lower than 1473 K at 1 GPa as reported by Yoshino et al. (2009)), various melt fractions were obtained using the same starting material. The resultant melt fraction increases with increasing temperature (Fig. 3). During the periods of t_2-t_4, it is found that the conductivity values of partially molten peridotite are nearly the same in three different principal directions (see Fig. S1 and Fig. 1b), and corresponding impedance spectra showed a complete semicircular at high frequencies and an additional part (tail) at low frequencies (Fig. 4); meanwhile, the absolute conductivity value for each run before the "zero time" of effective time (t_5) systematically increases with increasing temperature (or melt fraction) (Fig. 5). As the time t_5 prolongs and the shear deformation continues, the radius of the impedance arc obtained from shear (x) direction decreases with increasing effective time (Fig. 4a). In contrast, the radius of the impedance arc normal (y) to shear direction on the shear plane remains almost constant throughout the effective time (Fig. 4b). However, the radius of the impedance arc perpendicular (z) to the shear plane increases with the effective time (Fig. 4c). As a result, we observed that shear-parallel (x) conductivities increased rapidly by half to one order of magnitude and then remained constant for the duration of the experimental run (Fig. 5). In contrast, the conductivity normal (y) to shear direction on the shear plane remained constant, whereas z-direction conductivity decreased slightly and finally kept almost constant (Figs. 4 and 5). Consequently, 0.5-0.8 logarithmic unit ($\Delta[\log\sigma]_{xy}$)

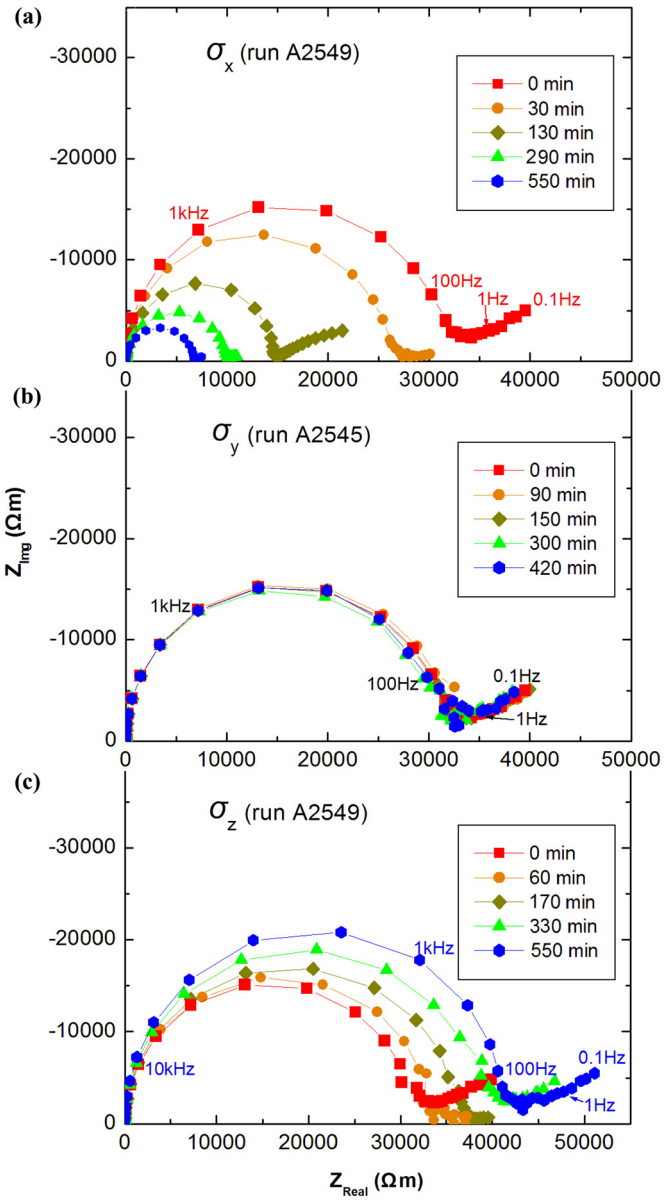

Fig. 4. Evolutions of representative impedance spectra of the deformed partially molten KLB-1 peridotite with effective time at 1498 K. (a) σ_x (run A2549). (b) σ_y (run A2545). (c) σ_z (run A2549).

difference between shear-parallel (x) and shear-normal (y) conductivity was observed, and the conductivity difference $\Delta[\log\sigma]_{xz}$ is around 0.8-1.0 logarithmic unit (Fig. 6a).

Although the magnitude of conductivity anisotropy is different, which may depend on temperature and strain rate, the development trends of conductivity anisotropy among different runs nearly trace the same path (Fig. 6a) after the onset of sample deformation. This observation implies that development of conductivity anisotropy is controlled by the increment rate of absolute conductivity. Nonetheless, the conductivity anisotropy did not appear at similar shear strain (Fig. 6b), even though various shear strains ($\gamma = 0.66\sim1.75$) have been generated in this study (Table 2).

3.2. Microstructural observations of deformed peridotite

Without shear deformation (or shear stress), melt distribution was homogeneous and most melt pockets was found at triple junc-

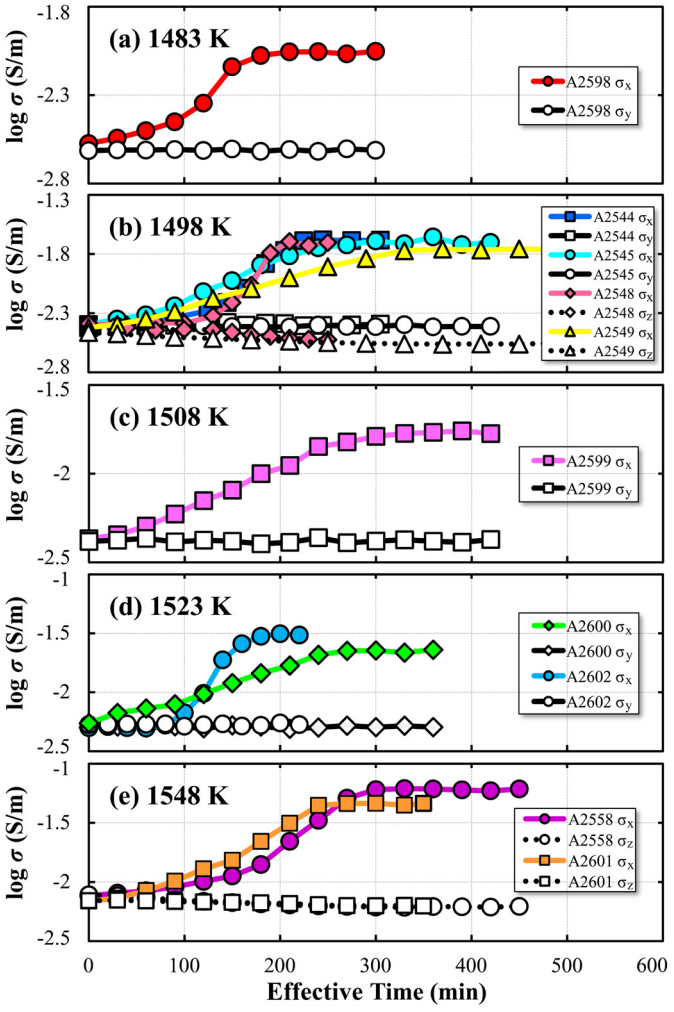

Fig. 5. In situ electrical conductivity of partially molten KLB-1 peridotites varies with effective time at different temperature. (a) 1483 K, (b) 1498 K, (c) 1508 K, (d) 1523 K, and (e) 1548 K. Note that the time corresponding to the point 2 (Fig. 1b) in this study was defined as "zero time" of effective time for shear deformation, where conductivity anisotropy begins to appear at point 2 due to pronounced anisotropic melt redistribution.

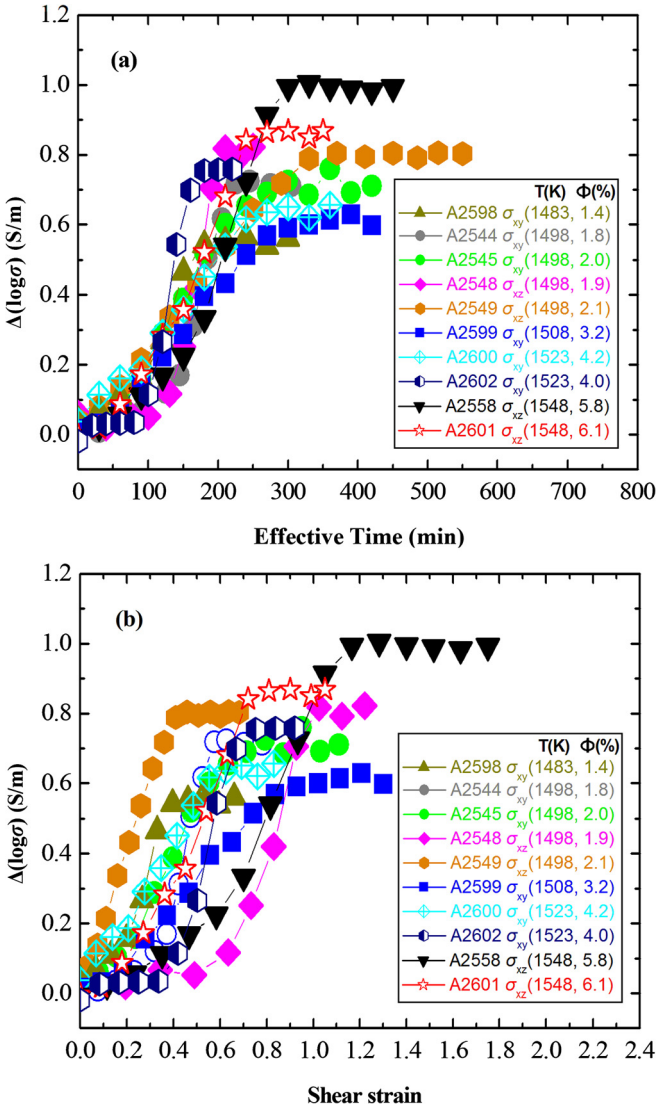

Fig. 6. Conductivity anisotropy [$\Delta(\log\sigma)$] of partially molten KLB-1 peridotites under shear deformation as a function of time (a) and shear strain (b). $\Delta(\log\sigma)$ is defined as the difference between logarithmic conductivity parallel (x) and normal (y) to the shear direction in the shear plane. The $\Delta(\log\sigma)$ of melt-bearing samples increases with time and strain. The conductivity values parallel (x) to the shear increase with increasing time for shear deformation, whereas those normal (y) to the shear are almost constant. In contrast, the conductivities perpendicular (z) to the shear plane decrease slightly.

tions composed of three olivine crystals, whereas melt was rare in the pyroxene-rich area (Fig. S2 in Supplementary Material). Fig. 7 shows results of the optical and BSE image analysis from the polished section of the deformed sample parallel to the shear direction (xz plane). Shear deformation leads to redistribution of melt from random distribution along the grain edge or grain boundary to aligned melt pockets with a strong MPO. Although both the composition and fraction of melt changed at each target temperature (Tables 1 and 2, Fig. 3 and Figs. S3-S4 in Supplementary Material), melt distribution of the deformed samples has similar characteristics irrespective of shear strain ($\gamma = 0.66\sim1.75$) (Table 2). Melt segregation occurred over the scale of several grains and two melt-rich regions parallel to the shear plane developed, which were separated by a melt-depleted region (Fig. 7c). The variation of melt fraction normal to the shear plane shows two sharp peaks in Fig. 7d, which is consistent with textural observation. The melt fraction in the central part of melt-rich region is distinctly higher ($\phi > 20$ vol.%) than that of the sample edge or center melt-depleted regions. The localizations of these two melt-rich regions occurred at regions adjacent to the sample-piston boundaries. In the melt-rich region, melt pockets preferentially occupied grain boundaries parallel to the shear direction and were elongated in the shear direction (Fig. 7e and f). On the polished section normal to the shear direction (yz plane), melt pockets are isolated (Fig. 7h and Figs. S5i-S5h in Supplementary Material), indicating no MPO (Fig. 7g). Although temperature conditions of each run are different, the melt distributions of the deformed samples indicated that two melt-rich regions were developed in a similar manner for all samples and finally aligned parallel ($\sim0°$) to shear direction regardless of temperature, melt composition and shear strain (Figs. S5-S6). In addition, it is found that the two melt-rich areas are not interconnected to each other in the normal (z) to the shear direction (Fig. 7c and Figs. S5-S6 in Supplementary Material).

4. Discussion

4.1. Effect of evolving melt composition on electrical conductivity

The Na and K are important charge carriers in silicate melt (Ni et al., 2011) and thus the electrical conductivity of melt is significantly influenced by alkali content. Roberts and Tyburczy (1999)

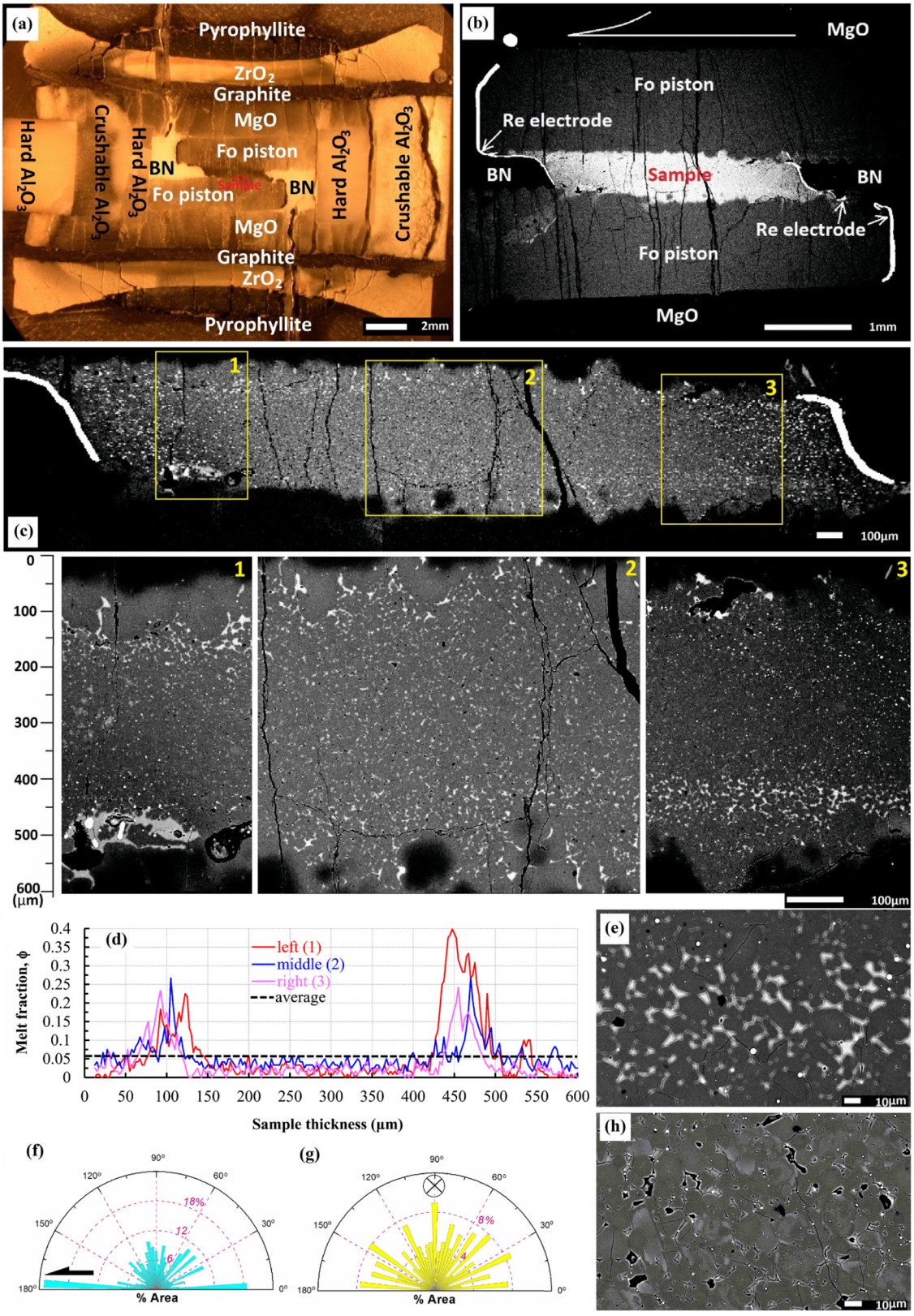

Fig. 7. Optical and back-scattered electron images of partially molten KLB-1 sample (A2601) with $\phi = 0.061$ melt, deformed to 105% shear strain. (a) Overview optical image of the shear deformed sample between two forsterite single-crystal pistons on the polished section, which is parallel to the shear direction and normal to the shear plane. The grooves on the forsterite piston can be seen at contact with BN. (b) BSE image of the polished section in the same orientation as (a), at a higher magnification. Note that the Re electrodes were inclined by shear deformation. (c) Whole sample image. Numbers and yellow boxes indicate the magnified portions. (d) Melt distribution as a function of the sample thickness. Note that two peaks appear at the upper and lower boundary, which suggested that melt segregation occurred and formed two melt-rich regions parallel to the shear direction, separated by one melt-depleted region. (e) BSE image shows that melt pockets were elongated in the shear direction. (f) Orientation of the long axis of melt pockets (MPO) as a percentage of the total melt area when viewed in a section cut parallel (*xz* plane) to the shear direction. (h) BSE image of the section cut normal (*yz* plane) to the shear direction shows melt pockets are isolated and without shape preferred orientation (g). Over 1000 individual melt pockets were measured for each graph in (f) and (g).

investigated the effect of melt chemistry on electrical conductivity in basaltic melt, showing an increase in conductivity with increasing alkali and Fe + Mg contents and with decreasing silica content. Our results show that Mg number slightly increases with temperature (Fig. S4a), while Na_2O contents (K_2O content is too low in Fig. S3 so its influence is insignificant) in recovered melts decrease with increasing temperature (Table 1 and Fig. S4b in Supplementary Material). As illustrated in Fig. S4, although the Na_2O content varies widely (1.91-2.55 wt.% in Fig. S4b) at 1498 K ($\phi \sim 0.02$), the changes of shear-parallel conductivities (σ_x) before and after shear deformation do not exceed 0.15 log units (Fig. S4c), as well at 1548 K (Na_2O = 1.26-1.77 wt.%). On the other hand, Yoshino et al. (2009) showed that the incipient melt with higher silica content has larger dihedral angle than basaltic melt. The worse wetting properties originated from the low degree of melting could reduce conductivity at the same melt fraction compared with basaltic melt case. At the same time enhancement of conductivity due to the high alkali content would be offset. These observations suggest that the electrical conductivity of partially molten KLB-1 peridotite is not dominantly controlled by alkali content in partial melt.

4.2. Effect of shear stress on melt topology

The present study demonstrates that the melt fraction of partially molten deformed peridotite systematically increases with increasing temperature. The feature of the melt distribution observed in this study is very similar to those in peridotite analog (Zhang et al., 2014). However, this texture is clearly different from those in partially molten rocks during deformation in torsion (Holtzman et al., 2003; Kohlstedt and Holtzman, 2009; Pommier et al., 2015). Most of previous experiments indicated that melt segregates into distinct melt-rich bands oriented ~20° antithetic to the macroscopic shear plane. As discussed in Zhang et al. (2014), this discrepancy should be attributed to different geometry for deformation experiments. The cylindrical piston cut at an angle of 90° in this study, whereas the cut angle was 45° adopted in the most previous studies.

Shear deformation of partially molten rock induces topological changes by a redistribution of melt from the equilibrium melt geometry that is established by annealing under hydrostatic stress conditions (see Fig. S2 in Supplementary Material). The microstructure developed in the sheared partially molten peridotite samples provides an excellent insight on framework for understanding the mechanisms by which the MPO develops. It is well known that the melt in undeformed peridotite is homogeneously distributed in grain boundary and triple junction (von Bargen and Waff, 1986), and displays no MPO (Fig. S2). The time variation of conductivity during deformation of partially molten system (Fig. 5) should reflect a change of the electrical anisotropy developing parallel to the shear direction, suggesting a textural transition from a homogenous distribution to a strong MPO parallel to the shear direction. However, one of the most remarkable textural features commonly observed in the deformed samples is an enhancement of grain boundary wetting (Holtzman et al., 2003; Kohlstedt and Holtzman, 2009). In this study, the degree of MPO does not appear to be controlled by total strain because strong MPO was found in all deformed samples (Fig. 2a, Fig. 7e-f and Figs. S5-S7 in Supplementary Material). These observations suggest that the development of MPO is caused by differential stress (Takei, 2010). In the laboratory, melt segregation is mainly driven by deviatoric stress rather than surface tension (Holtzman et al., 2003; Kohlstedt and Holtzman, 2009; Zhang et al., 2014). We note that the electrical conductivity increases rapidly in the first tens of minutes and appeared reaching near steady-state within one hour even if shear deformation maintains. It implies that the anisotropic interconnectivity of the melt can be mostly achieved within a few hours (Fig. S1 and Fig. 1). Once shear deformation started, impedance spectroscopy measurements and the microstructural analyses of samples clearly indicated that stress-induced melt redistribution is responsible for the observed electrical anisotropy within the effective time (Figs. 4-7). Due to strain partitioning between melt-rich and -poor bands, shear stress gradient will further draw melt into regions with higher melt fractions and form melt-rich regions. The generation of such bands would enhance the melt connectivity and the electrical conductivity in the shear direction. These observations suggest that the development of conductivity anisotropy was caused by the realignment of partial melt parallel to the shear direction. The time required for the development of conductivity anisotropy was longer for runs with a relatively lower strain rate (Figs. 5 and 6a), depending on the strain rate. In addition, the magnitude of conductivity anisotropy became constant for each deformation run independently of shear strain (Fig. 6b), suggesting that shear strain is not a main controlling factor for development of the conductivity anisotropy.

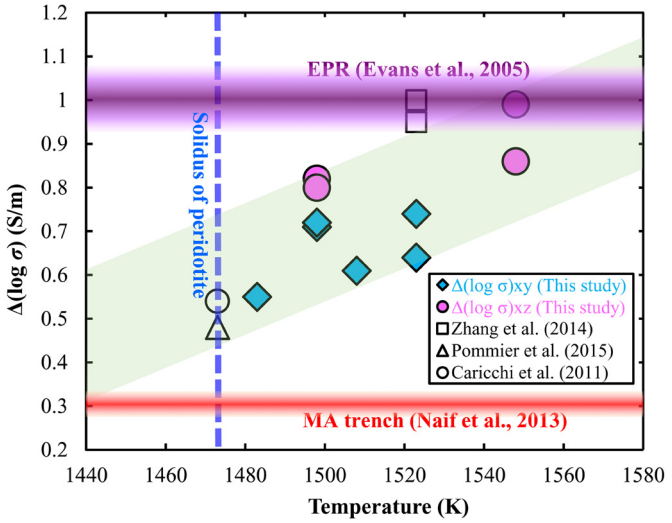

Fig. 8. Comparison of laboratory data on electrical anisotropy ($\Delta(\log\sigma)$) of partially molten KLB-1 peridotite as a function of temperature with the geophysically observed electrical anisotropy in the oceanic asthenosphere beneath the oceanic plate. The purple and red regions represent the magnitude of electrical anisotropy near the East Pacific Rise (Evans et al., 2005) and beneath the edge of the Cocos plate at the Middle America trench offshore of Nicaragua (Naif et al., 2013), respectively. The light green shadow indicates the trend of $\Delta(\log\sigma)$ with temperature for partially molten peridotite obtained in this study. The dashed blue line shows the solidus temperature of peridotite with KLB-1 composition at 1 GPa.

4.3. Effect of temperature on the electrical conductivity anisotropy

The total melt fraction acquired for peridotite increased from 1.8 to 6.1 vol.% when temperature increases from 1483 to 1548 K (Fig. 3). The absolute conductivity values in three principal directions increase with increasing temperature, as well as the magnitude of conductivity anisotropy in the different directions ($\Delta[\log\sigma]_{xy}$ and $\Delta[\log\sigma]_{xz}$) (Figs. 6 and 8 and Table 2), suggesting that the development of conductivity anisotropy is significantly controlled by an increase of temperature. On the other hand, the conductivities normal (y) to shear direction on the shear plane and/or perpendicular (z) to the shear plane remained constant or slightly decreased during annealing at a given temperature, which implies that the melt connectivity became worse perpendicular to the shear direction (Kohlstedt and Holtzman, 2009; Caricchi et al., 2011; Zhang et al., 2014). Since development of the electrical conductivity anisotropy and increase of shear-parallel (x) conductivity were caused by the elongation of melt pockets parallel to the shear direction. To better understand the nature of

anisotropic distribution of the melt due to melt segregation, we have estimated how much melt fraction is partitioned into melt-rich regions by calculating the area ratio of two melt-rich regions to the whole area in Fig. S5g and Fig. 7d (more details given in Appendix B). Our analysis shows that once melt segregation occurs, more than 50% of the total melt fraction will partition into the two melt-rich regions at 1498 K (Fig. S5g), and this proportion continuously increases with increasing temperature. This observation may suggest that the magnitude of electrical anisotropy of partially molten KLB-1 peridotite is not simply estimated as a function of the total melt fraction.

4.4. Comparison with previous studies

Experimental measurement on the electrical conductivity of partially molten peridotites under shear deformation is a challenging task because of technical difficulties. A comparison of the present results on the electrical conductivity of partially molten peridotite with some previous studies is shown in Fig. S8. Caricchi et al. (2011) did the first experimental measurement on melt-bearing olivine aggregates in torsion to detect development of electrical anisotropy during shear deformation. Their results showed that electrical conductivity perpendicular to the shear direction reduced during deformation of melt-bearing (4.4 and 11.2 vol.% basalt) olivine aggregates at 1473 K. It is worth noting that only one direction (y) was measured in experiment of Caricchi et al. (2011) and the conductivities normal (y) to shear direction decreased during deformation, whereas σ_y remain constant in our studies (Zhang et al., 2014 and this study). This may be because the existence of large shear stress gradients in their experiment would further decrease the connectivity of the melt along the measurement direction, thus reducing the conductivity (Fig. S8).

Zhang et al. (2014) performed the conductivity measurement on olivine + chromite/enstatite aggregates with basaltic melts simultaneously in two directions of three principal axes: parallel and normal to the shear direction on the shear plane, and perpendicular to the shear plane. They suggested that horizontal electrical conductivity anisotropy revealed by magnetotelluric surveys in the oceanic asthenosphere can be well explained by the realignment of the sheared peridotite analog with 2 vol.% of partial melt induced by shear stress. Although the experimental setup is same between Zhang et al. (2014) and this study, it is found that the magnitude of conductivity anisotropy ($\Delta(\log\sigma) \approx$ 1-1.5) in peridotite analog under similar experimental conditions (P, T, strain rate) reported by Zhang et al. (2014) were larger than those observed in this study ($\Delta(\log\sigma) \approx$ 0.55-0.95), and previous works ($\Delta(\log\sigma) <$ 0.6) (Caricchi et al., 2011; Pommier et al., 2015) (Fig. S8 and Fig. 8). This discrepancy may be mainly caused by the different starting materials used in these works (partially molten lherzolite (KLB-1): this study, peridotite analog: Caricchi et al., 2011; Zhang et al., 2014; Pommier et al., 2015). Remarkably, Yoshino et al. (2005) have shown that the grain boundary wetness of the liquid from the partially molten lherzolite (KLB-1) is significantly lower than that of the olivine-basalt system because of different melt composition and mineralogy. Especially, the presence of pyroxenes in partially molten lherzolite inhibits the formation of apparently wetted boundaries between pyroxenes and olivine (Toramaru and Fujii, 1986; Zhu et al., 2011).

Pommier et al. (2015) performed electrical anisotropy measurements on the pre-deformed olivine aggregates and pre-sheared partially molten rocks fairly below the melting temperature of peridotite. Their results indicated that samples with 5 vol.% MORB and 2 vol.% carbonate yield similar conductivity values at 1473 K, and no systematic effect of shear strain ($1.2 < \gamma < 9$) on conductivity was observed for melt-bearing samples. These observations are consistent with experimental investigations in this study and Zhang et al. (2014). However, one important finding in Pommier et al.'s experiment is that the electrical conductivity anisotropy decreases with increasing temperature and then become negligible at high temperature, which is contrary to our observations in this study. This difference can be attributed to the technical problems. Pommier et al. (2015) measured the electrical conductivity of pre-sheared partially molten peridotite analog under quasi-hydrostatic condition rather than under shear deformation. As a result, their conductivity measurements displayed a quick rearrangement of melt from anisotropic distribution to a nearly isotropic melt distribution with increasing temperature within short period because of the removal of shear stress. In contrast, our method can allow monitoring the development of electrical anisotropy associated with the evolution of anisotropic melt-rich networks during shear deformation. Furthermore, as shown in Fig. S8 and Fig. 8, the magnitude of conductivity anisotropy in the partially molten lherzolite observed in this study increases with increasing temperature or melt fraction. We should note that all previous works (Caricchi et al., 2011; Zhang et al., 2014; Pommier et al., 2015) were conducted at fixed melt fraction and temperature. Therefore, these experiments are unlikely to evaluate the effects of melt fraction and temperature on the evolution of conductivity anisotropy in partially molten systems during shear deformation.

4.5. Implications for electrical anisotropy in the oceanic upper mantle

Due to constraints on the limited time of high pressure experiments, laboratory deformation experiments must be performed at strain rates that are much faster compared to those appropriate for flow processes in the mantle (10^{-4}-10^{-6} s^{-1} versus 10^{-12}-10^{-14} s^{-1}) (Kohlstedt and Holtzman, 2009). Experiments are usually carried out at differential stresses higher than those found in the mantle (tens of MPa-a few GPa versus 0.1-1 MPa). It is necessary to extrapolate laboratory results to mantle conditions. For samples to achieve textural equilibrium or attain a steady-state microstructure in the laboratory environment, fine-grained (grain size $<$ 20 μm) samples are often used so that the effective diffusion distance is relatively shorter. Shear deformation experiments on partially molten rocks (Holtzman et al., 2003; Holtzman and Kohlstedt, 2007; Kohlstedt and Holtzman, 2009; Caricchi et al., 2011; Zhang et al., 2014; Pommier et al., 2015) have demonstrated that a melt preferred orientation develops at the grain scale and melt segregation into a network of melt-enriched bands occurs at a large scale. In the laboratory, melt migration, segregation, and organization are likely to be driven by gradients in shear stress associated with regional variations in viscosity rather than surface tension (Kohlstedt and Holtzman, 2009). At low shear stresses, surface tension should be a significant driving force and contribute to melt redistribution toward an isotropic configuration to achieve the minimum interfacial energy in the system. However, the bulk contribution of surface tension to the melt distribution decreases with increasing grain size (Holtzman and Kohlstedt, 2007). In the asthenosphere, differential stress would dominate over surface tension such that stress-driven melt segregation can occur when we consider the large grain size in the region (Holtzman et al., 2003; Holtzman and Kohlstedt, 2007; Kohlstedt and Holtzman, 2009).

Near the East Pacific Rise (EPR), MT surveys (Evans et al., 2005; Baba et al., 2006) reported two important features of the electrical conductivity profile near a mid-ocean ridge. The conductivity largely increases with increasing depth from 50 to 100 km. It also becomes strongly anisotropic in this depth range. The difference of conductivities at 100 km between the direction parallel (10^{-1} S/m) and normal (10^{-2} S/m) to the plate motion reaches one order of magnitude (Fig. 8). In order to reach the magni-

tude of the electrical anisotropy (~1 log units), temperature estimated from partially molten peridotite is higher than 1498 K in this study. The degree of electrical anisotropy in partially molten KLB-1 peridotite at 1498 K is more than 0.8 log units (if consider $\Delta(\log\sigma)_{xz}$), which is consistent with the electrical anisotropy reported by Evans et al. (2005) and Baba et al. (2006), as well as experimental data (Zhang et al., 2014). The electrical anisotropy near the EPR is unable to account for by low temperature of 1473 K (Caricchi et al., 2011; Pommier et al., 2015) (Fig. 8). On the other hand, the present experimental results (Fig. 8 and Fig. S9) suggested that more than 2 vol.% (at 1498 K) of total melt fraction for partially molten peridotite is required to explain the electrical anisotropy revealed by MT surveys (Evans et al., 2005; Baba et al., 2006), which agrees with those (~2 vol.%) inferred previously (Caricchi et al., 2011; Zhang et al., 2014) but remarkably smaller than that (~5 vol.%) estimated by Pommier et al. (2015). This discrepancy should be attributed to the different experimental strategy used in this study and previous works.

As shown in Fig. 8 and Fig. S9, the conductivity anisotropy corresponding to its magnitude observed beneath near the EPR can develop even at low melt fraction (~2 vol.%) by melt redistribution. However, higher temperature is required to explain the absolute conductivity values. At a low degree of melting of fertile peridotite at 1 GPa, chemical composition of incipient melt is significantly different from those of typical basaltic melts (e.g., Baker and Stolper, 1994; Baker et al., 1995), as well as the wetness of the partially molten peridotite (Yoshino et al., 2005). In fact, significant evolution of melt composition with temperature was also found in this study (Table 1). Electrical conductivity is sensitive to chemical composition of partial melt (e.g., Roberts and Tyburczy, 1999; Pommier et al., 2008), especially when the peridotite contains volatile components (Gaillard et al., 2008; Yoshino et al., 2010, 2012; Sifré et al., 2014). The electrical response of volatile-bearing partial molten silicates is expected to have the maximum value at very low degree melting. In contrast, the melt conductivity would have much smaller compositional dependence since chemical composition of volatile-free peridotite becomes higher alkali content (Na and K) rising conductivity and SiO_2 contents reducing conductivity with decreasing temperature. The estimation of melt fraction from the conductivity values requires accurate knowledge of petrology. Furthermore, development of anisotropic melt distribution by shear deformation makes it more difficult to estimate melt fraction. Consequently, the potential melt fraction in the upper mantle may have been misestimated in previous studies without considering the effect of evolving melt chemistry and melt distribution. The present study shows that the conductivity of partial molten peridotite simply increases with increasing temperature and melt fraction (Figs. 3 and 8). The fact that this tendency matches volatile-free case implies that higher temperature (> 1523 K) and the resultant higher melt fraction (~5 vol.%) are necessary to explain both the conductivity anisotropy and values beneath near the EPR (Fig. S9).

Beneath the Cocos plate at the Middle America trench, Naif et al. (2013) revealed high conductivity anomalies confined to depths of 45 to 70 km in the asthenosphere, whereas only a small anisotropy ($\sigma_{max}/\sigma_{min} \approx 3$) is observed despite the high speed of the plate motion (8.5 cm/yr). Our in-situ conductivity measurements indicate that the magnitude of the electrical conductivity anisotropy in the partially molten KLB-1 peridotite increases with increasing temperature (see light green shadow region in Fig. 8 and Table 2) or increases with increasing melt fraction (see light blue arrows in Fig. S9). Clearly, the experimental results of this study, as well as previous investigations (Caricchi et al., 2011; Zhang et al., 2014; Pommier et al., 2015), are unable to account for the small anisotropy (only 0.3 log units) beneath the Cocos plate (Fig. 8). In order to realize small anisotropy, lower temperature condition is required; for example, the temperature is estimated to be 1445 K based on the present experimental investigations, whereas this temperature is under the solidus temperature of peridotite (Takahashi, 1986; Yoshino et al., 2005) and the absolute conductivity at this temperature is also one order lower than that observed by MT data. On the other hand, in order to reach the absolute high conductivity value (~$10^{-0.5}$ S/m) in Fig. S9, higher temperature (> 1560 K) is required so that higher melt fraction (~9 vol.%) and larger conductivity anisotropy (1.4 log units) are produced, which is inconsistent with small magnitude of anisotropy (0.3 log units) reported by Naif et al. (2013). Previous studies have demonstrated that the volatile components (H_2O and CO_2) can significantly increase melt conductivity (e.g., Gaillard et al., 2008; Ni et al., 2011; Yoshino et al., 2010, 2012; Sifré et al., 2014) and decrease melting temperature (Green et al., 2010; Hirschmann, 2010; Dasgupta et al., 2013). Therefore, one reasonable explanation for the high conductivity anomalies but with a small anisotropy observed under the Cocos plate at the Middle America trench (Naif et al., 2013) is that this region has low melt fraction but containing high concentration of volatile components, as suggested by Naif et al. (2013). Even at lower temperatures, the melt containing more H_2O and CO_2 components can account for high conductivity and the small magnitude of anisotropy, because the electrical conductivity of hydrous carbonated basalt is higher by at least one order of magnitude than that of hydrous basalt (Ni et al., 2011; Yoshino et al., 2010, 2012; Sifré et al., 2014).

Petrology experiments demonstrated that incipient melting can occur at 100-150 km depth, even deeper ~410 km, initially assisted by volatiles (e.g., Hirschmann, 2010; Green et al., 2010; Dasgupta et al., 2013; Sifré et al., 2014). When the upwelling materials reach ~100 km, melting occurs without the help of volatiles and the degree of melting increases substantially leading to the dehydration of residual minerals (Green et al., 2010). As a result, the following picture can be established (Kohlstedt and Holtzman, 2009; Hirschmann, 2010): melt produced in asthenosphere would migrate upward along grain boundaries, and would ultimately accumulate at the base of a less permeable lithosphere. Excessive melt accumulation at 70-100 km depth may lead to rheological weakening, enhanced shear deformation and finally formation of sub-horizontal melt-rich layers (Kawakatsu et al., 2009) that can well explain a sharp high-velocity contrast and electrical anisotropy at the LAB. In this horizontal melt-rich layer, tube networks or elongated melt pockets shear into a network of interconnected melt-rich channels in the direction of plate motion, probably driven by large-scale asthenospheric flow. The development of melt-rich channel parallel to the plate motion largely contributes to the conductivity anisotropy, while the bad connectivity of melt perpendicular to the shear plane contributes to form melt-rich layer, leading a sharp decrease of shear velocity. Segregation and organization of melt during deformation may have important consequences for geodynamics, through their influences on rheological and transport properties. In a passively upwelling plate-spreading environment, strain rates are the highest in the zones of corner flow and increase toward the ridge axis. In the light of the viewpoint that stress-driven melt segregation and organization will be the most effective near the ridge, it is accepted that the LAB is marked by the location of melt-enriched shear zones that lubricate the LAB and thus the plate boundary system (Holtzman et al., 2003; Kohlstedt and Holtzman, 2009).

Declaration of competing interest

The authors declare no competing financial interests.

Acknowledgements

We thank editor J.P. Brodholt, M. Laumonier and one anonymous reviewer for their constructive comments that greatly improve the manuscript. This study was financially supported by Key Research Program of Frontier Sciences of CAS (ZDBS-LY-DQC015), NSF of China (41973056, 41773056, 41303048), Science Foundation of Guizhou Province (2017-1196, 2018-1176) and the 1000Plan Program for Young Talents to B.Z., and JSPS MEXT/KAKENHI (Grant Number JP15H05827, 17H01155) to T.Y. This study was performed using joint-use facilities of the Institute for Planetary Materials, Okayama University.

Appendix. Supplementary material

Supplementary material related to this article can be found online at https://doi.org/10.1016/j.epsl.2019.115922.

References

Baba, K., Chave, A.D., Evans, R.L., Hirth, G., Mackie, R.L., 2006. Mantle dynamics beneath the East Pacific Rise at 17°S: insights from the Mantle Electromagnetic and Tomography (MELT) experiment. J. Geophys. Res. 111, B02101. https://doi.org/10.1029/2004JB003598.

Baker, M.B., Stolper, E.M., 1994. Determining the composition of high-pressure mantle melts using diamond aggregates. Geochim. Cosmochim. Acta 58, 2811–2827. https://doi.org/10.1016/0016-7037(94)90116-3.

Baker, M.B., Hirschmann, M.M., Ghiorso, M.S., Stolper, E.M., 1995. Compositions of near-solidus peridotite melts from experiments and thermodynamic calculations. Nature 375, 308–311. https://doi.org/10.1038/375308a0.

Caricchi, L., Gaillard, F., Mecklenburgh, J., Le Trong, E., 2011. Experimental determination of electrical conductivity during deformation of melt-bearing olivine aggregates: implications for electrical anisotropy in the oceanic low velocity zone. Earth Planet. Sci. Lett. 302, 81–94. https://doi.org/10.1016/j.epsl.2010.11.041.

Dai, L.D., Karato, S., 2014. High and highly anisotropic electrical conductivity of the asthenosphere due to hydrogen diffusion in olivine. Earth Planet. Sci. Lett. 408, 79–86. https://doi.org/10.1016/j.eps1.2014.10.003.

Dasgupta, R., Mallik, A., Tsuno, K., Withers, A.C., Hirth, G., Hirschmann, M.M., 2013. Carbon-dioxide-rich silicate melt in the Earth's upper mantle. Nature 493, 211–215. https://doi.org/10.1038/nature11731.

Evans, R.L., Hirth, G., Baba, K., Forsyth, D., Chave, A., Mackie, R., 2005. Geophysical evidence from the MELT area for compositional controls on oceanic plates. Nature 437, 249–252. https://doi.org/10.1038/nature04014.

Gaillard, F., Malki, M., Iacono-Marziano, G., Pichavant, M., Scaillet, B., 2008. Carbonatite melts and electrical conductivity in the asthenosphere. Science 322, 1363–1365. https://doi.org/10.1126/science.1164446.

Gardés, E., Gaillard, F., Tarits, P., 2015. Comment to "High and highly anisotropic electrical conductivity of the asthenosphere due to hydrogen diffusion in olivine" by Dai and Karato [Earth Planet. Sci. Lett. 408 (2014) 79–86]. Earth Planet. Sci. Lett. 427, 296–299. https://doi.org/10.1016/j.epsl.2015.06.041.

Green, D.H., Hibberson, W.O., Kovács, I., Rosenthal, A., 2010. Water and its influence on the lithosphere-asthenosphere boundary. Nature 467, 448–451. https://doi.org/10.1038/nature09369.

Hirschmann, M.M., 2010. Partial melt in the oceanic low velocity zone. Phys. Earth Planet. Inter. 179, 60–71. https://doi.org/10.1016/j.pepi.2009.12.003.

Holtzman, B.K., Kohlstedt, D.L., Zimmerman, M.E., Heidelbach, F., Hiraga, T., Hustoft, J., 2003. Melt segregation and strain partitioning: implications for seismic anisotropy and mantle flow. Science 301, 1227–1230. https://doi.org/10.1126/science.1087132.

Holtzman, B.K., Kohlstedt, D.L., 2007. Stress-driven melt segregation and strain partitioning in partially molten rocks: effects of stress and strain. J. Petrol. 48 (12), 2379–2406. https://doi.org/10.1093/petrology/egm065.

Karato, S., 1990. The role of hydrogen in the electrical conductivity of the upper mantle. Nature 347, 272–273. https://doi.org/10.1038/347272a0.

Kawakatsu, H., Kumar, P., Takei, Y., Shinohara, M., Kanazawa, T., Araki, E., Suyehiro, K., 2009. Seismic evidence for sharp lithosphere–asthenosphere boundaries of oceanic plates. Science 324, 499–502. https://doi.org/10.1126/science.1169499.

Kohlstedt, D.L., Holtzman, B.K., 2009. Shearing melt out of the Earth: an experimentalist's perspective on the influence of deformation on melt extraction. Annu. Rev. Earth Planet. Sci. 37, 561–593. https://doi.org/10.1146/annurev.earth.031208.100104.

Laumonier, M., Farla, R., Frost, D.J., Katsura, T., Marquardt, K., Bouvier, A.S., Baumgartner, L.P., 2017. Experimental determination of melt interconnectivity and electrical conductivity in the upper mantle. Earth Planet. Sci. Lett. 463, 286–297. https://doi.org/10.1016/j.epsl.2017.01.037.

Naif, S., Key, K., Constable, S., Evans, R.L., 2013. Melt-rich channel observed at the lithosphere–asthenosphere boundary. Nature 495, 356–359. https://doi.org/10.1038/nature11939.

Ni, H., Keppler, H., Behrens, H., 2011. Electrical conductivity of hydrous basaltic melts: implications for partial melting in the upper mantle. Contrib. Mineral. Petrol. 162, 637–650. https://doi.org/10.1007/s00410-011-0617-4.

Poe, B.T., Romano, C., Nestola, F., Smyth, J.R., 2010. Electrical conductivity anisotropy of dry and hydrous olivine at 8 GPa. Phys. Earth Planet. Inter. 181, 103–111. https://doi.org/10.1016/j.pepi.2010.05.003.

Pommier, A., Gaillard, F., Pichavant, M., Scaillet, B., 2008. Laboratory measurements of electrical conductivities of hydrous and dry Mount Vesuvius melts under pressure. J. Geophys. Res. 113, B05205. https://doi.org/10.1029/2007JB005269.

Pommier, A., Leinenweber, K., Kohlstedt, D.L., Qi, C., Garnero, E.J., Mackwell, S.J., Tyburczy, J.A., 2015. Experimental constraints on the electrical anisotropy of the lithosphere-asthenosphere system. Nature 522, 202–206. https://doi.org/10.1038/nature14502.

Ringwood, A.E., 1975. Composition and Petrology of the Earth's Mantle. McGraw-Hill, New York, p. 618.

Roberts, J.J., Tyburczy, J.A., 1999. Partial-melt electrical conductivity: influence of melt composition. J. Geophys. Res. 104, 7055–7065. https://doi.org/10.1029/1998JB900111.

Shankland, T.J., Waff, H.S., 1977. Partial melting and electrical conductivity anomalies in the upper mantle. J. Geophys. Res. 82, 5409–5417. https://doi.org/10.1029/JB082i033p05409.

Sifré, D., Gardes, E., Massuyeau, M., Hashim, L., Hier-Majumder, S., Gaillard, F., 2014. Electrical conductivity during incipient melting in the oceanic low-velocity zone. Nature 509, 81–85. https://doi.org/10.1038/nature13245.

Takahashi, E., 1986. Melting of a dry peridotite KLB-1 up to 14 GPa: implications on the origin of peridotitic upper mantle. J. Geophys. Res. 91, 9367–9382. https://doi.org/10.1029/JB091iB09p09367.

Takei, Y., 2010. Stress-induced anisotropy of partial molten rock analogue deformed under quasi-hydrostatic loading test. J. Geophys. Res. 115, B03204. https://doi.org/10.1029/2009JB006568.

Toramaru, A., Fujii, N., 1986. Connectivity of melt phase in a partially molten peridotite. J. Geophys. Res. 91, 9239–9252. https://doi.org/10.1029/JB091iB09p09239.

von Bargen, N., Waff, H.S., 1986. Permeabilities, interfacial areas and curvatures of partially molten systems: results of numerical computations of equilibrium microstructures. J. Geophys. Res. 91 (B9), 9261–9276. https://doi.org/10.1029/JB091iB09p09261.

Wang, D., Mookherjee, M., Xu, Y., Karato, S., 2006. The effect of water on the electrical conductivity of olivine. Nature 443, 977–980. https://doi.org/10.1038/nature05256.

Weeraratne, D.S., Forsyth, D.W., Yang, Y., Webb, S.C., 2007. Rayleigh wave tomography beneath intraplate volcanic ridges in the South Pacific. J. Geophys. Res. 112 (B6), B06303. https://doi.org/10.1016/2006JB004403.

Yang, X.Z., 2012. Orientation-related electrical conductivity of hydrous olivine, clinopyroxene and plagioclase and implications for the structure of the lower continental crust and uppermost mantle. Earth Planet. Sci. Lett. 317–318, 241–250. https://doi.org/10.1016/j.epsl.2011.11.011.

Yoshino, T., Takei, Y., Wark, D.A., Watson, E.B., 2005. Grain boundary wetness of texturally equilibrated rocks, with implications for seismic properties of the upper mantle. J. Geophys. Res. 110, B08205. https://doi.org/10.1029/2004JB003544.

Yoshino, T., Matsuzaki, T., Yamashita, S., Katsura, T., 2006. Hydrous olivine unable to account for conductivity anomaly at the top of the asthenosphere. Nature 443, 973–976. https://doi.org/10.1038/nature05223.

Yoshino, T., Yamazaki, D., Mibe, K., 2009. Well-wetted olivine grain boundaries in partial molten peridotite in the asthenosphere. Earth Planet. Sci. Lett. 283, 167–173. https://doi.org/10.1016/j.epsl.2009.04.007.

Yoshino, T., Laumonier, M., Mclsaac, E., Katsura, T., 2010. Electrical conductivity of basaltic and carbonatite melt-bearing peridotites at high pressures: implications for melt distribution and melt fraction in the upper mantle. Earth Planet. Sci. Lett. 295, 593–602. https://doi.org/10.1016/j.epsl.2010.04.050.

Yoshino, T., Mclsaac, E., Laumonier, M., Katsura, T., 2012. Electrical conductivity of partial molten carbonatite peridotite. Phys. Earth Planet. Inter. 194–195, 1–9. https://doi.org/10.1016/j.pepi.2012.01.005.

Yoshino, T., Katsura, T., 2013. Electrical conductivity of mantle minerals: role of water in conductivity anomalies. Annu. Rev. Earth Planet. Sci. 41, 605–628. https://doi.org/10.1146/annurev-earth-050212-124022.

Zhang, B.H., Yoshino, T., Yamazaki, D., Manthilake, G., Katsura, T., 2014. Electrical conductivity anisotropy in partially molten peridotite under shear deformation. Earth Planet. Sci. Lett. 405, 98–109. https://doi.org/10.1016/j.epsl.2014.08.018.

Zhu, W., Gaetani, G.A., Fusseis, F., Montési, L.G., De Carlo, F., 2011. Microtomography of partially molten rocks: three-dimensional melt distribution in mantle peridotite. Science 332, 88–91. https://doi.org/10.1126/science.1202221.